Sensors & Diagnostics

PAPER

View Article Online
View Journal | View Issue

Cite this: *Sens. Diagn.*, 2025, **4**, 856

A digital nonenzymatic nucleic acid amplification assay for ultrasensitive detection of cell-free microRNA in human serum

Tao Yu,[a] Aditi Dey Poonam,[a] Amy Halbing,[b] Shengwei Zhang,[a] Yingmiao Liu,[c] Zheng Li,[a] William Marx,[a] Andrew B. Nixon[c] and Qingshan Wei *[a]

Received 25th April 2025,
Accepted 28th July 2025

DOI: 10.1039/d5sd00057b

rsc.li/sensors

Few point-of-care (POC) molecular methods exist that are as sensitive as polymerase chain reaction (PCR) while maintaining the simplicity, portability, and robustness for detecting specific nucleic acids in complex sample media. Here, we developed an isothermal nonenzymatic amplification cascade, named sequential nonenzymatic amplification (SENA), and its digital assay version (dSENA), for the ultrasensitive detection of cell-free microRNAs (miRNAs) in diluted human serum with a >95% recovery rate. SENA consists of two layers of DNA circuit-based amplifiers, in which the hybridization chain reaction (HCR) and catalyzed hairpin assembly (CHA) were concatenated to amplify the signals by more than 4000-fold. The sensitivity was further improved in dSENA, where a limit of detection (LOD) down to 5 fM was achieved under the optimized conditions. SENA and dSENA together demonstrated a broad detection dynamic range over 6 logs of analyte concentrations (10 fM – 10 nM), and high specificity for discriminating target miRNAs from point mutations and other interference sequences. dSENA was demonstrated to quantify expression levels of miR-21 and miR-92 in colorectal cancer patient serum with accuracy comparable to RT-PCR. Given its simplicity, compactness, and PCR-like performance, SENA holds great potential in POC miRNA or ssDNA analysis.

Introduction

MircoRNAs (miRNAs) are a family of small non-coding RNA molecules with 18–25 nucleotides, which play essential roles in gene expression by translational repression or degradation of messenger RNAs.[1–3] Recently, studies have shown that cell-free miRNAs (or circulating miRNAs) can stably exist in extracellular human body fluids, including blood plasma, urine, and saliva.[4,5] Their existence in blood has attracted great attention due to their potential as noninvasive biomarkers for the diagnosis of various diseases such as cancer, cardiovascular disease, brain and liver injury.[6,7] However, detection of circulating miRNA remains a great challenge because of their short sequences, high degree of sequence similarity, and low abundance in blood. The commonly used approaches, such as northern blotting[8] and reverse transcription-polymerase chain reaction (RT-PCR)[9,10] are complicated to operate and therefore have limited their applications in the laboratory settings. While enzyme-catalyzed amplification methods like RT-PCR offer high detection sensitivity, they are labor-intensive and require specialized instrumentation such as thermocyclers for precise thermal cycling, which significantly increases operational costs and reduces point-of-care (POC) accessbility.[11,12] Additionally, the reliance on protein-based enzymes necessitates a cold chain for storage and transportation due to their temperature sensitivity and limited shelf life, further hindering large-scale field deployment.[13] Detection of small RNA targets such as microRNAs is also challenging for PCR-based methods, as their short sequence length restricts primer design (typically 15–30 nucleotides in length) and can limit amplification efficiency.[14] Alternatively, a number of signal amplification strategies employing nanomaterial[15,16] or enzyme labels[17] have recently been developed for the detection of low abundant miRNAs. However, their inherent drawbacks of complicated protocols and high cost still cannot meet the criteria for POC miRNA testing.

To address the need for POC diagnostics, various nonenzymatic nucleic amplification strategies have been developed for detecting miRNAs. Many of these methods are based on the DNA circuit amplifiers, such as homogeneous entropy-driven hybridization,[18] hybridization chain reaction (HCR),[19–21] and catalyzed hairpin assembly (CHA),[22,23] which do not involve any enzyme molecules or polymerases, and thus eliminate the need for cold storage of reagents and significantly

[a] *Department of Chemical and Biomolecular Engineering, North Carolina State University, 911 Partners Way, Campus Box 7905, Raleigh, NC 27695, USA. E-mail: qwei3@ncsu.edu*
[b] *Department of Biological Sciences, North Carolina State University, 112 Derieux Place, Raleigh, NC 27695, USA*
[c] *Department of Medicine, Duke University Medical Center, Durham, NC 27710, USA*

reduce assay costs. However, current implementations of nonenzymatic nucleic acid detection reactions are usually limited by their amplification power. The fold amplification (defined as the number of output signals divided by input nucleic acid targets) of the most DNA circuit strategies is still less optimal (typically less than 1000-fold) compared to the conventional PCR (typically 10^8–10^{10} fold).[24,25] A strategy to circumvent such limitation is to construct multi-layer DNA circuits in a single reaction, which can significantly improve the limit of detection (LOD) of DNA circuit amplifiers to the low picomolar (pM) level.[26–32] For example, Ellington *et al.* (2012) reported a format of hybrid assay using stacked toehold-mediated strand displacement circuits (HCR-CHA or stacked CHA), which yielded 7000-fold signal amplification for two-layer circuits and 600 000-fold for four-layer cascades.[33,34] Later, Wang *et al.* (2016) have successfully engineered a two-layer CHA-HCR amplification cascade. The signal was gained through Förster resonance energy transfer (FRET), and a LOD down to 1 pM was achieved.[35] A CHA-HCR detection assay was also developed by Wang *et al.* (2018), wherein the CHA products generated in response to target miRNA acted as initiators for downstream HCR amplification, achieving a detection limit of 2 pM.[36] Similarly, Li *et al.* (2022) used palindrome-based HCR (PHCR) with CHA to detect miR-21, with a target detection limit of 10 pM.[37] Wei *et al.* (2016) also combined CHA and HCR, in which miR-144 first initiated HCR reaction that further triggered the CHA process, reaching an impressive LOD of 0.3 fM.[38] However, the reactions require sequential incubations (first with HCR reactants, followed by the addition of CHA components), totaling over 3 hours, with a lack of testing on clinical samples. This multi-step protocol limits its suitability for rapid or POC applications, where one-pot reactions are preferable. Recently, Li *et al.* (2025) introduced a split-free, enzyme-free autocatalytic DNA circuit (SAA) that mimics PCR's three-step cycle, to achieve exponential amplification of target DNA. Using hairpin-mediated strand displacement reactions, the circuit produces newly synthesized target replicates without enzymes or thermal cycling. However, the detection limit achieved by the platform was only in the low picomolar level (9.2 pM).[39]

Another general strategy to improve the detection sensitivity of a molecular assay is to convert the analog signals into digital outputs.[40,41] Digital molecular assays bring a new level of precision in quantifying nucleic acids by partitioning the bulk sample solutions into microscale chamber arrays, so that each partition well contains a discrete number of biological entities (*e.g.*, 0, 1, 2, 3, *etc.*). The concentration of analytes is quantified by counting positive partition wells, where each microwell reports a digital result of a single-molecule event (1, positive and 0: negative).[41,42] In that case, the digital assay is superior to conventional bulk assay in detection sensitivity. In addition, the digital assay format could also reduce the required sample volumes and the overall footprint of the assay to facilitate POC use. Digital assay readout has been extensively implemented in PCR (*e.g.*, digital droplet or microwell-based PCR),[43–47] isothermal amplification approaches such as LAMP[48–50] and ELISA.[51,52] However, there are few reports on the digital nonenzymatic reactions.[53,54] One of the reasons may be due to the design of DNA circuits is relatively more complicated than other commonly miniaturized methods such as PCR or LAMP. On the other hand, different from temperature-controlled reaction (*e.g.*, PCR and LAMP), most entropy-driven DNA circuits are instant reactions. That means signal leakage should be considered in the process of forming the digital compartment.

Here, we introduce a new digital nonenzymatic amplification assay utilizing two-layers of hybrid DNA circuit reactions for the detection of miRNAs with an optimized sensitivity approaching the PCR method. The ultimate goal is to provide a compact and ultrasensitive solution to facilitate POC applications towards trace-level biomarker detection. The method is termed sequential nonenzymatic amplification (SENA), accompanied by its digital variation dSENA. SENA consists of both HCR and CHA amplification circuits in a simple reaction pot. In this study, the assay conditions have been systematically optimized to achieve an amplification power of >4000 fold for SENA and a LOD of 5 fM for dSENA. Such LOD of dSENA is on the same order of magnitude as that (1.7 fM) of quantitative PCR (qPCR), and much lower than most currently available nonenzymatic amplification methods.[26–37] Combining both analog and digital readouts, a total linear dynamic range of 6 orders of magnitude was achieved for SENA and dSENA together, which meets the needs of most clinical diagnostic applications. While we demonstrated the performance of SENA and dSENA for highly sensitive detection of cell-free miR-21 in human serum, similar analog/digital nonenzymatic assays also could be scaled to detect other targets such as small molecules, DNAs, and proteins by introducing proper target recognition units. Therefore, dSENA integrates the advantages of enzyme-free amplification assays of operating at isothermal conditions and stable reagents at ambient temperature with the high analytical sensitivity characteristic of RT-PCR, achieving detection limits in the low femtomolar range. As such, the proposed strategy could be a universal one-pot POC assay platform, which is extremely useful for the detection and quantification of low copy number biomarkers.

Results and discussion

Assay principle

Fig. 1A depicts the working principle of the SENA assay, which includes stacked HCR-CHA amplification cascades and a turn-on fluorescent signal generation mechanism. In this design, the nonenzymatic amplification cascades are performed in two steps: first, the HCR reactions are triggered upon exposure to miR-21, where two hairpins (H1 and H2, see sequences in Table S1) are cross-opened and self-assembled into elongated HCR products. During this process, the toeholds of H1 and H2 are co-localized along with the HCR products, forming *M* copies of double flaps (Fig. 1A, Step 1). Second, the co-localized double

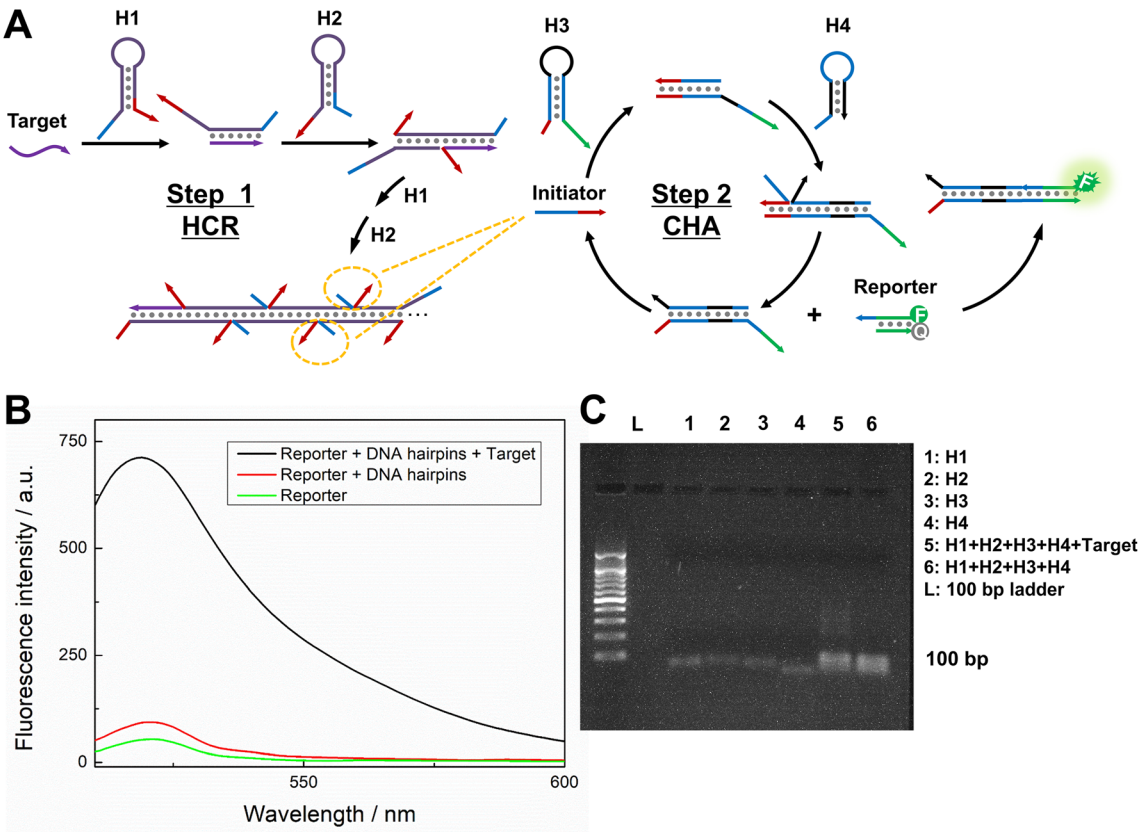

Fig. 1 (A) Schematic illustration of the principle of the two-layered SENA assay for cascaded detection of miR-21. (B) Fluorescent emission spectra of the SENA assay under different conditions. The full-component assay (black curve) consisted of 100 nM H1/H2, 500 nM H3/H4, 500 nM reporter, and 5 nM miR-21. (C) Gel electrophoresis analysis (2% agarose) of different assay components and products: lane L, 100 bp ladder; lane 1, 500 nM H1; lane 2, 500 nM H2; lane 3, 500 nM H3; lane 4, 500 nM H4; lane 5, a mix of all four hairpins (500 nM H1/H2 and 500 nM H3/H4) and 50 nM target; and lane 6, a mix of all four hairpins without targets (500 nM H1/H2 and 500 nM H3/H4).

flaps will serve as the initiator sequences to trigger sequential CHA reactions, which introduce catalytic assembly of the other two hairpins (H3 and H4) in a looped amplification cycle to form N copies of final products – an opened hairpin assembly with a hanging activated toehold for signal generation (Fig. 1A, Step 2). Finally, to ease signal readout and quantification by a portable reader device, a turn-on and wash-free fluorescence signal generation mechanism has been implemented. After completion of two-step reactions, the CHA products are reacted with molecular beacon reporters, where the quencher sequences (Q) are separated and displaced, and the fluorophore-conjugated sequences (F) are hybridized to the CHA products to produce N copies of turned-on fluorescent molecules (Fig. 1A). The entire process is able to generate a total amplification power of $M \times N$ in theory. The initiators are the key elements that link the two DNA circuit amplifiers. The initiator sequences are split into two segments (blue and red sequences, in Fig. 1A) and are conjugated to the termini of both H1 and H2. Part of initiator sequences is protected in the stems (6 bases total) of H1/H2, so that H1/H2 alone will not trigger the CHA cascades. As a result, the SENA assay is able to have all reaction components (4 hairpins plus a DNA reporter) pre-mixed, and run to complete isothermally upon exposure to miR-21 targets.

The proof-of-concept demonstration of the proposed SENA assay for sensitive detection of miR-21 was first validated by detecting the fluorescent signal change of the assay with and without target analytes (Fig. 1B). In the absence of miR-21, the SENA reagent mixture (4 hairpins + DNA reporter) showed a comparable fluorescent emission at 520 nm (red curve, Fig. 1B) to that of DNA reporter alone (green curve, Fig. 1B), which is considered as an acceptable background. However, upon adding the target miR-21 (5 nM), the fluorescent emission peak centered at 520 nm increased significantly (black curve, Fig. 1B). These initial results confirm that the hairpin mix can stably co-exist in the solution, and the amplification cascades can be triggered by the introduction of miR-21 sequences. The cascade reaction products were then characterized by agarose gel electrophoresis. As shown in Fig. 1C, from left to right, it could be observed that each hairpin formed a single band (lane 1 to lane 4). When target miR-21 was added to the complete hairpin mixture (lane 5), the original hairpin bands disappeared. Instead, a new smeared band with a broad range of molecular weight was formed from 50 bp to over 1 kbp as well as a solid band around 100 bp appeared (lane 5). These indicate that HCR and CHA reactions were taken place in the presence of target miR21 and raw hairpin reactants were exhausted. The

smeared band is attributed to the products of HCR reaction, which produces long nicked dsDNA-like polymers with widely distributed lengths and therefore molecular weights. The solid band on the other side is attributed to the CHA duplex products (Fig. 1A). In contrast, when the target is absent, the mixture of four hairpins (H1 + H2 + H3 + H4) did not generate a similar gel smear, suggesting no DNA circuit reactions occurred (Fig. 1C, lane 6). Moreover, incomplete assay combinations, such as H1 + H2, H3 + H4, and H1 + H2 + target, did not produce a positive result either (Fig. S1). These results confirm that the two-layer HCR + CHA reaction occurs only if all assay components as well as the target are present.

Optimization of assay conditions

To minimize DNA circuit leakage (*i.e.*, spontaneous cascade reactions in the absence of targets) and achieve the optimal performance for detecting miR-21, the assay conditions of SENA, such as the number of initiator bases protected in the stem, the molar ratio of HCR hairpins (H1/H2) to CHA hairpins (H3/H4), and the reaction time, were systematically optimized. In order to prevent H1/H2 hairpins (both containing initiator fragments at terminals) from triggering CHA reactions, we embedded a few bases of initiator sequences into the stem sections of H1/H2 hairpins (named "stem-protected bases"). We designed three types of H1/H2 hairpins with different numbers of stem-protected bases (0, 3, and 6) to investigate the effectiveness of suppressing background signal and leakage. As shown in Fig. 2A, compared with protected hairpins (3 or 6 protected bases, red and blue lines, respectively), nonprotected hairpins (*i.e.*, initiator segments directly attached to the terminals of H1/H2 hairpins) showed a much higher background signals even in the absence of targets ([miR-21] = 0 pM) in the solution (black line). The protective effect seems proportional to the length of initiator bases being included in the stem, where 6-base protected hairpins exhibited the lowest background fluorescence at zero analyte concentration (Fig. 2A, blue line). Furthermore, the turn-on fluorescence signals increased as a function of target concentrations for all cases. When the miR-21 concentration reached 500 pM, all three types of hairpins showed a similar level of end-point fluorescence intensity, indicating that introduction of protection bases (3 or 6 bases) into the stem of H1/H2 hairpins did not impede the cross-opening and self-assembly of H1 and H2, but it significantly suppressed spontaneous circuit leakage. Therefore, for the best assay signal-to-noise ratio (SNR), we

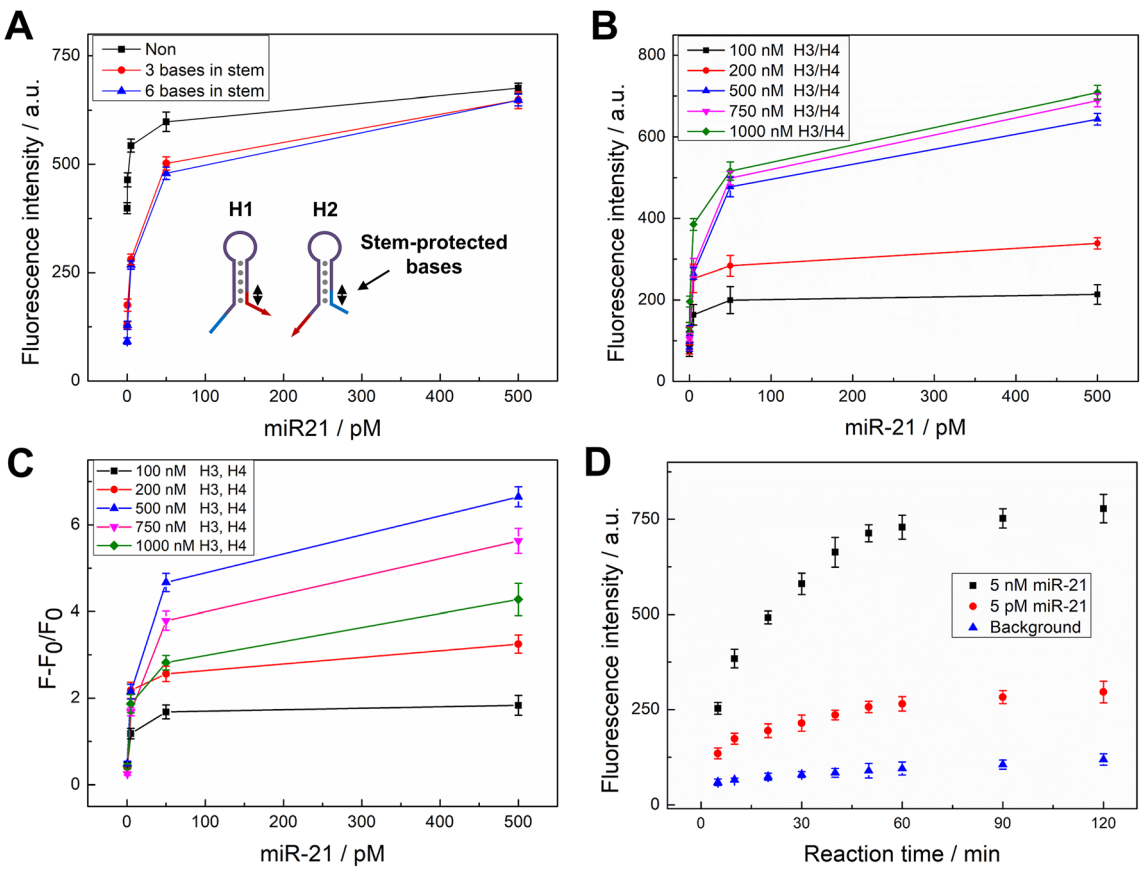

Fig. 2 Optimization of SENA assay conditions. (A) Effect of numbers of stem-protected bases in H1/H2. (B and C) Effect of stoichiometric ratios of H1/H2 and H3/H4; (B) represents raw fluorescence intensities and (C) is after background normalization. (D) Effect of reaction time. The concentrations of H1/H2 and H3/H4 were set at 100 nM and 500 nM, respectively. The reporter DNA was at 500 nM.

used 6-base protected H1/H2 hairpins for all subsequent experiments.

Second, the influence of different stoichiometric ratios between H1/H2 and H3/H4 was investigated. To do that, the concentrations of H1/H2 hairpins and DNA reporters were fixed at 100 nM and 500 nM, respectively. Then, different concentrations of H3/H4 hairpins were added to investigate the impact on the fluorescent signal recovery. As shown in Fig. 2B, with the increase of concentrations of H3/H4 from 100 to 1000 nM, the detected fluorescent intensities of the assay also increased proportionally. However, the concentration of H3/H4 also modulated the background fluorescence intensity. We then used an analytical parameter, the percent of fluorescence increase, to exclude the background fluctuation and quantify the true impact of H3/H4 concentrations on the overall assay signals. The percent of fluorescence increase is defined by $(F–F_0)/F_0$, where F is the detected fluorescence intensity with analytes and F_0 represents the background fluorescence intensity without analytes. After normalization, the results in Fig. 2C showed that 500 nM H3/H4 produced the highest fluorescent signals for a broad range of analytes tested (blue curve). A concentration of H3/H4 hairpins at 500 nM seems the optimal condition, because higher concentrations of H3/H4 may cause the increase of background signals, while lower concentrations of H3/H4 led to insufficient reactants for the following CHA reactions. As such, 500 nM H3/H4 hairpins were used for all future tests unless otherwise mentioned.

Moreover, the kinetics of the SENA assay was also investigated by monitoring the fluorescence intensity increase over time. The time-dependent fluorescence intensities of the assay with or without miR-21 were shown in Fig. 2D. In the presence of 5 pM and 5 nM miR-21, the assay signals elevated quickly during the initial stage and then slowly increased after 60 min (black and red line). 60 min appeared to be the optimal reaction time for the amplification reaction to approach the equilibrium state. On the other side, the background fluorescence signal in the absence of targets did not change significantly over time (blue line), confirming no severe nonspecific leakage reaction again. Taken all together, we used 100 nM H1/H2, 500 nM H3/H4, 500 nM reporter, 6-base protected H1/H2, and 60 min reaction as the optimal conditions for all following experiments.

Detection sensitivity and specificity

Using the optimized assay conditions, the LOD of the SENA assay for the detection of target miR-21 was quantified. Fig. 3A shows representative fluorescence spectral responses of the assay corresponding to a series of diluted concentrations of miR-21 (from 0.2 pM to 5 nM). The fluorescence intensity at 520 nm gradually increased with the increase of miR-21concentration. The peak intensity at 520 nm was then plotted against the miR-21concentration, showing a rapid signal increase for miR-21 concentrations between 0.2 pM to 500 pM (Fig. 3B). By plotting the fluorescence intensity *versus* the logarithmic concentration of miR-21, a calibration curve was obtained over the range from 0.2 pM to 5 nM (inset of Fig. 3B). The LOD was quantified to be 0.12 pM by finding the corresponding miR-21 concentration, where its assay signal is above 3× of the standard deviation of the blank (inset of Fig. 3B).

SENA's high detection sensitivity is attributed to the engineered architecture of two-layers of amplification reactions (HCR-CHA) in a simple mixture pot. Compared with single-layer CHA reaction (Fig. S2A–C), the LOD has been improved by ~240 times from 29 pM in CHA to 0.12 pM in SENA. We further compared the amplification power between CHA and SENA, where the amplification power (AP) is defined as:

$$\mathrm{AP} = \frac{\#\text{ of signal molecules with analyte} - \#\text{ of signal molecules without analyte}}{\#\text{ of analyte}}$$

In SENA, the signal molecules generated through the amplification reaction are essentially the CHA duplex products

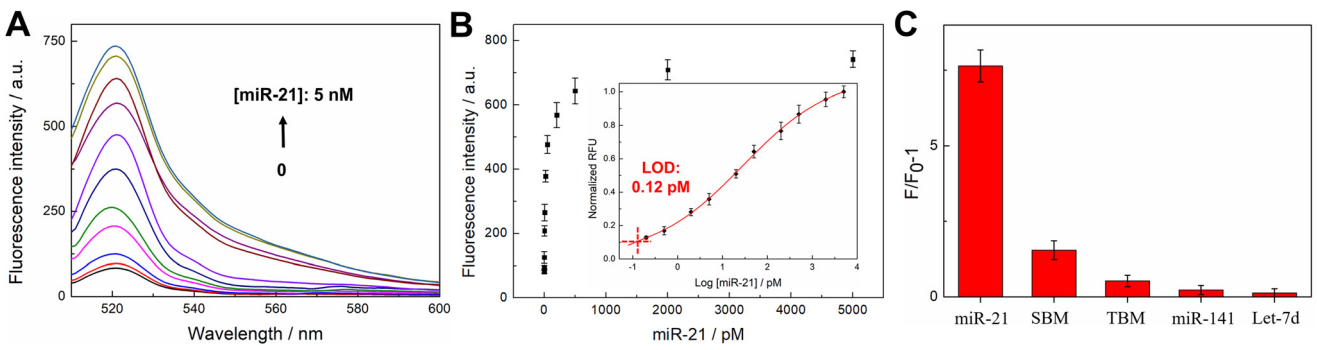

Fig. 3 Quantification of LOD and detection specificity. (A) Fluorescent emission spectra of the SENA assay in the 96-well plate in response to different concentrations of miR-21 (from bottom to top: 0, 0.2, 0.5, 2, 5, 20, 50, 200, 500, 2000, and 5000 pM). (B) Peak fluorescent intensity at 520 nm *versus* different concentrations of miR-21. Error bars represent the standard deviation of three measurements. (C) Specificity test of the SENA assay. miR-21 and its mutations (SBM and TBM) were tested at 5 nM, whereas other control miRNAs (miR-141 and let-7d) were tested at 50 nM. SBM: single-base mutation; TBM: triple-base mutation.

(Fig. 1A). The correlation between the number of signal molecules and fluorescent intensities was established in a control experiment by mixing stimulate signal sequences with the reporter molecules (Fig. S3). Using that calibration, the # of signal molecules with and without analytes can be estimated by measuring the fluorescent signals of the assays before and after adding the analytes, respectively. The peak amplification power of CHA (Fig. S2D) is calculated to be around 80-fold for analyte ranging from 50 to 500 pM, which agrees well with previously reported amplification fold numbers in the literature.[20] In contrast, the SENA assay amplifies signals by more than 4000-fold (Fig. S4), approximately 50 times better than the conventional CHA approach.

To validate the specificity of SENA assay, single-base mutation (SBM) and triple-base mutation (TBM) sequences of miR-21, miR-141, and let-7d were used as control sequences to challenge the assay reaction (see detailed sequences in Table S1). The concentrations of miR-141 and let-7d were 10 times higher than miR-21, while its mutations (SBM and TBM) were tested at equal concentrations. As shown in Fig. 3C, SBM is the most interfering agent among the sequences being tested, which generated about 20.4% of signals compared to miR-21. In contrast, the signal of TBM is only about 7.11% of that of miR-21, much less than SBM; moreover, miRNA-141 and let-7d generated negligible fluorescent signals (<2.92%). This comparison clearly shows that this approach has a high selectivity against other control miRNAs and their mutations, which can offer potential applications to discriminate target miRNAs from their close family members and other interference sequences.

Construction of a digital SENA (dSENA) assay

To eventually develop a POC and field-deployable diagnostic assay for individuals, we next adapted the tube-based SENA assay into a microfluidic digital assay platform (digital SENA, or dSENA) to further improve its detection sensitivity, portability, and readability by cost-effective optical sensors such as smartphone-based readers. Miniaturization of SENA assay into a chip format will also simplify and automate the reaction process, which is highly desired for diagnostics in the field or resource-limited settings.

In our design, a microarray pattern was prepared in polydimethylsiloxane (PDMS) through a standard photolithography protocol (see Methods). As shown in Fig. 4A and B, a PDMS chip consists of 9 microarrays; Each microarray is about 2 × 2 mm in size and contains 100 × 100 microwells, which are 13 μm in diameter and 15 μm in height. The SEM image showed the uniformity of the fabricated cylindrical microwell chambers (Fig. 4B, inset). The volume of each microwell is ~2 pL, and the minimum sample volume required for each PDMS chip is ~0.12 μL. Oxygen plasma treatment was applied to reduce the hydrophobicity of PDMS surface and facilitate the wetting of the microwells by liquid solutions before sampling loading (Fig. S5). After treatment, each microarray can be uniformly loaded with a low volume of samples driven directly by the capillary force (Fig. 4C).

The operation of the dSENA assay is relatively simple without the need for expensive laboratory equipment. As shown in Fig. 4D, a droplet of reaction solution (including all hairpins and reporters) was first placed on the glass substrate and then mixed with a sample droplet (containing miRNA). The mixture was then quickly sandwiched between the PDMS and glass layers by employing a gentle pressure on the top of the PDMS layer to evacuate excess liquid and gas bubbles. The Van der Waals force was sufficient to bond the PDMS sheet to the surface of a glass slide to seal individual microwells.[40] We noticed such a process generated a very

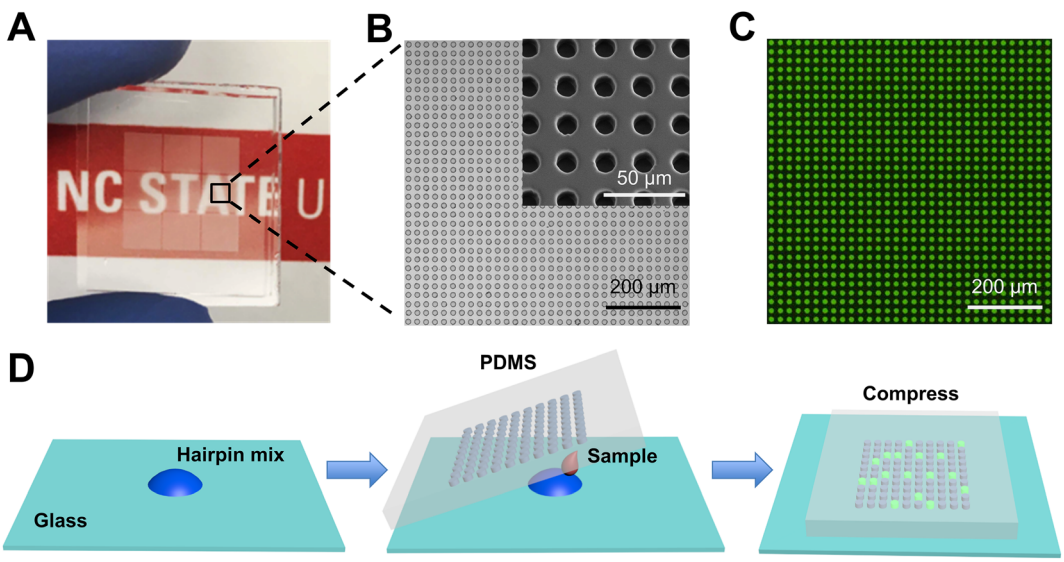

Fig. 4 Illustration of formation steps for the dSENA assay. (A) Photograph of the digital microfluidic chip used for the analysis of miR-21. (B) Brightfield microscopy image of the microwell array. Inset: SEM image of the microwell array. (C) Fluorescent image of the microwell array filled with 100 nM FAM dye. (D) Schematic illustration of the basic operation steps of dSENA. From left to right: step 1, add reagent solution that contains hairpin probe mix and reporters; step 2, add analyte solution, and step 3, compress to seal.

homogeneous distribution of small molecules among thousands of independent reaction microwells (Fig. 4C). Compared with the traditional pump/valve-based array chips, which would take minutes to more than an hour for sample loading and sealing, our compression-based sample sealing process is much simpler and faster (completed in seconds), making it ideally suited for POC use. After sealing the microarray chip, the cascade reaction was performed at 37 °C for 1 h. The chip was then transferred to an inverted fluorescence microscope equipped with a 4× objective lens for digital counting of positive wells.

The principle of digital assay relies on the observation of single-molecule reactions in individual reaction wells when the analyte concentration is extremely low. Following the Poisson distribution, the concentration of analytes (c) is proportional to the fraction of positive wells (f), which can be described by:

$$-\ln(1-f) = v\ c\ x_{dil}N$$

where v is the volume of microwell (2 pL), c is the concentration of miRNA (pM), x_{dil} is the diluted factor, and N is the Avogadro's number (see methods).

To test the performance of dSENA, we performed the digital assay for various concentrations of miR-21, ranging from 0 fM to 1 pM. The representative fluorescence images of the digital assay are shown in Fig. 5A. As the target concentration increased, more and more positive microwells were observed from the fluorescence images. The bright microwells are randomly distributed, indicating a uniform sample partition across the digital chip. The fraction of positive wells increased from 0.2% to 43.9%, when the concentration of miR-21 increased from 2 fM to 1 pM (Fig. 5A). Theoretically, the fraction of positive wells will increase to 63.2%, when the chip is saturated with single-molecule events (one analyte per well, or λ = 1, λ = (# of analytes)/(# of microwells)). In this regard, the test concentrations are well below the saturation concentration so that the Poisson statistics is valid for the entire concentration range that has been tested. The experimental relationship between the concentration of miR-21 and the calculated fraction of positive wells (Fig. 5B, black curve) followed exactly the theoretical prediction based on Poisson statistics (Fig. 5B and S6, blue curve). Each experimental data point was tested three times independently by using three newly prepared digital chips. By plotting the logarithm of positive

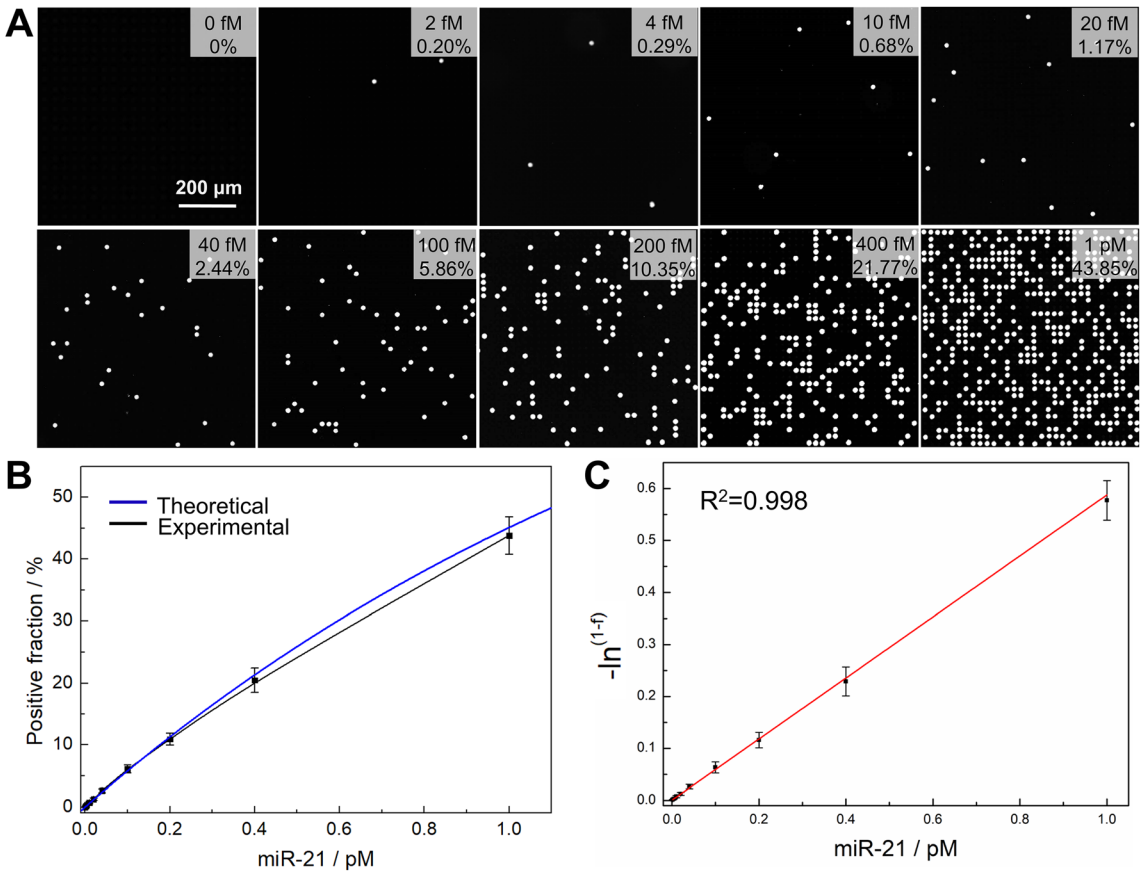

Fig. 5 Performance of the dSENA assay. (A) Fluorescence images of dSENA with different concentrations of miR-21. The percentage of positive microwells of each experiment is shown in the top right corner. (B) Positive fraction as a function of the concentration of miR-21. The blue curve represents the theoretical prediction obtained from the Poisson statistics. The black curve is the actual experimental measurement. (C) A linear regression curve of miR-21, by plotting –ln(1 – f) against the concentration of miR-21.

faction against the concentration of miR-21, a linear calibration curve was obtained (Fig. 5C).

Comparison of SENA, dSENA, and quantitative PCR (qPCR)

Furthermore, the performance of developed nonenzymatic assays (SENA and dSENA) was side-by-side compared with conventional gold standard amplification methods such as quantitative PCR (qPCR, or real-time PCR). As shown in Fig. 6A and B, the LODs of dSENA and SENA for miR-21 are 5 fM and 120 fM, respectively. The digital assay improved the detection sensitivity by approximately 24 times when compared with its analog counterpart. As expected, the dynamic range of dSENA has been entirely shifted to the lower analyte concentration range and is narrower than the analog SENA assay. The qPCR assay, on the other side, demonstrated a combination of excellent detection sensitivity and dynamic range (Fig. 6C). A LOD of 1.74 fM was achieved for qPCR, which is on the same order of magnitude with dSENA. These results indicate that the constructed digital nonenzymatic assay clearly outperforms analog nonenzymatic assay. The detection sensitivity of dSENA is also approaching the conventional qPCR, which is quite encouraging given its simplicity, cost-effectiveness, and potential for POC use since no enzyme molecules and thermal cycles are needed in dSENA to initiate the amplification reaction.

Detection of miR-21 in diluted human serum and dry reagent test

Next, both SENA and dSENA assays were tested for detection of miR-21 in a more complicated sample environment such as human serum to show the robustness of the methods for clinical applications. Briefly, the healthy human serum samples were diluted 50, 20, and 10 times, and spiked with different concentrations of miR-21 (Fig. 6D). The recovery rate of the assay is defined as the ratio of measured miR-21 concentration/spiked miR-21 concentration. For the SENA assay, the spiked miR-21 concentrations (0.5, 5, 50 pM) were slightly higher than those used for the dSENA assay (20, 100, 500 fM). All spiked concentrations are above the LOD of corresponding assays. The recovery rate of miR-21 was maintained above 90% for both SENA and dSENA assays for analyte concentrations from 20 fM to 50 pM being tested (Fig. 6D). Both assays performed slightly better in more diluted serum samples (*e.g.*, 50×) than less diluted controls (*e.g.*, 10×), which is due to reduced interference from serum proteins in more diluted samples. dSENA is particularly more robust to nonspecific interference from sample matrices, as evidenced by little difference in recovery

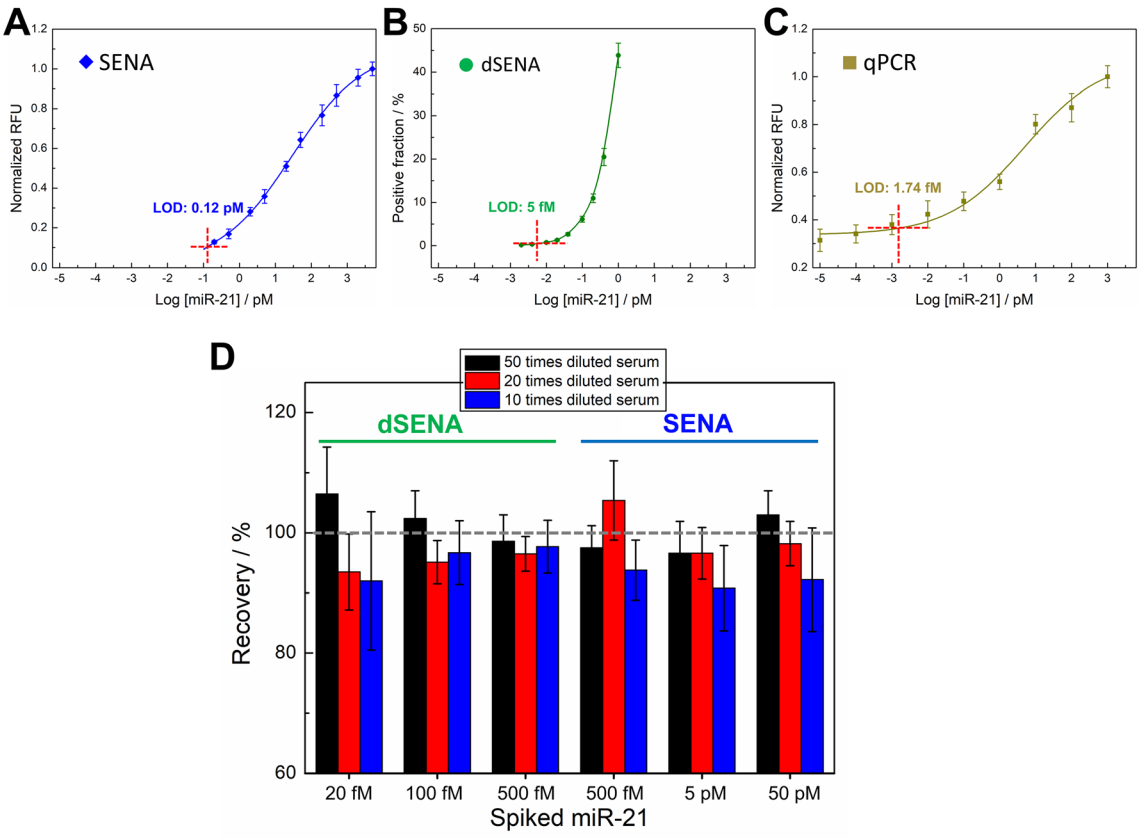

Fig. 6 Comparison of the performance of (A) SENA, (B) dSENA, and (C) qPCR in the detection of miR-21. The LOD is 120 fM for SENA, 5 fM for dSENA, and 1.74 fM for the qPCR assay, respectively. (D) Detection of miR-21 in human serum by SENA and dSENA. The recovery rates were calculated for human serum diluted by 50 times (black bar), 20 times (red bar), and 10 times (blue bar). Error bars are mean ± SD.

rates for different dilution factors when detecting 100 or 500 fM of targets. Both assays maintained their performance (>90% recovery rate) for dilution factors as small as 10×, which is advantageous over many other conventional molecular assays that usually require several steps of sample purification, including dilution.

Moreover, the performance of SENA and dSENA was investigated by using fully dehydrated (dry) reagents on the chip to represent the final POC format for miR-21 detection in diluted serum samples. The hairpin mixture and reporters were first dried on a 96-well plate (analog assay) or glass substrate (digital assay), and then rehydrated by adding the spiked serum samples to complete the reaction. The recovery results of digital and analog assays were summarized in Table S2. The recovery of miR-21 ranged from 95.0% to 104.4%, indicating that both SENA and dSENA can be well performed even using the dried reagent format. This represents another unique advantage of nonenzymatic assays, whose reaction components can be conveniently pre-dried on the chip devices for easy transportation and storage.

Quantification of miRNA in colorectal cancer (CRC) patient samples with dSENA chip

Finally, to investigate the reliability of dSENA chip in analyzing real clinical samples, the expression levels of miR-21 and miR-92 in serum samples of CRC patients were detected with the dSENA chip and standard RT-PCR. As shown in Fig. 7A and B, dSENA measurements indicated the up-regulated expression of miR-21 (Fig. 7A) and miR-92 (Fig. 7B) in all CRC patient samples tested (see the digital image in Fig. S8), which are consistent with the results provided by RT-PCR (Fig. 7C and D) and reported literature.[55,56] A ROC statistical analysis was further conducted to quantitatively evaluate the clinical accuracy of the dSENA results compared to RT-PCR (Fig. S9). For miR-21, the dSENA platform achieved an AUC of 0.94, while RT-PCR reached 0.98. For miR-92, AUCs were 0.89 and 0.96 for dSENA and RT-PCR, respectively. The high AUC values (approaching 1) indicate clinically relevant levels of diagnostic discrimination between CRC patients and healthy controls. The above results thus clearly demonstrate that the developed dSENA biochip is highly reliable for serum circulating miRNA detection, closely matching RT-PCR, suggesting its potential in the analysis of low-abundance biomarker molecules in real clinical samples. It is worth mentioning that the stability of dSENA assay components is dependent on the sample matrix. The hairpin structures are very stable in the standard buffer or 10% human serum samples at 37 °C (Fig. S10). Slight reaction leakage was observed in 50% human serum without any targets (Fig. S10, lane 3). This suggests a proper dilution of human serum is needed for the best assay results for real sample applications.

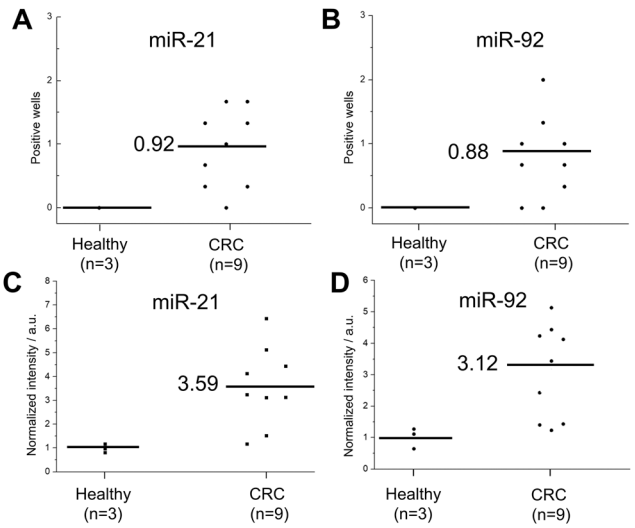

Fig. 7 Quantification of miR-21 and miR-92 in clinical CRC patient samples by the dSENA chip (A and B) and RT-PCR (C and D). Each dot represents the average value of three independent measurements.

Conclusion

In summary, we have demonstrated a nonenzymatic dual-layer amplification strategy, SENA and its digital format dSENA, with substantial signal gain for highly sensitive detection of miR-21 biomarkers. This hybrid isothermal amplification assay takes the advantage of both HCR and CHA, and its performance was systematically optimized by investigating the structure of hairpin stems, the stoichiometric ratio of reaction components, and the reaction kinetics. The method was able to amply signals by more than 4000-fold in the tube-based assay and enabled detection of miR-21 down to 5 fM in the digital chip format, approaching the qPCR detection sensitivity. Besides, the method also showed high selectivity for discriminating miR-21 from its mutation sequences and other miRNA biomarkers. The assay was also robust enough to work in high concentration serum samples (10× dilution) as well as dried state, and recovery rates of miR-21 detection in human serum were between 90.8% and 106.5% for all samples tested. Finally, a good agreement of miRNA expression level quantification was achieved in real CRC patient samples when comparing sSENA to RT-PCR as the gold standard. This field-friendly, robust, and sensitive method may find numerous applications for POC diagnostics, such as circulating cell-free nucleic acid sensing in clinical samples.

Methods

Chemicals and apparatus

All the chemicals (including human serum) were obtained from Sigma-Aldrich (MO, USA, analytical grade) and used without further purification or modification. PDMS was purchased from Sylgard 184, Dow Corning (MI, USA). 10× PCR buffer, 10× TBE buffer, Reverse transcriptase, dNTPs, Taq DNA polymerase, and SYBR green dye were purchased from Thermo Fisher Scientific (MA, USA). Silicon wafer was purchased from Wafer Universe (MA, USA). Ultrapure water (18.3 MΩ cm) was produced by Milli-Q system (Millipore, Inc., USA) and used throughout the experiments. All of the oligonucleotides used in this work were

synthesized and purified by Integrated DNA Technologies (Coralville, IA, USA). The sequences of the DNA and microRNA molecules are listed in Table S1.

Fluorescent spectra were recorded on a multi-mode microplate reader (SpectraMax M2, Molecular Devices). Scanning electron microscope (SEM) images were obtained on an FEI Verios 460 L scope, using an accelerating voltage of 2 kV. Fluorescent images were captured on an inverted microscope (IX83, Olympus, Japan) and a 4× objective lens (NA 0.7). Microfluidic chips were designed by Adobe Illustrator and fabricated by OAI's exposure system (CA, USA).

Nonenzymatic miR-21 amplification assay

All DNA strands and miRNA were stored in 10 mM Tris-HCl buffer (pH 7.5) at 10 μM concentrations in −20 °C refrigerator, and pre-warmed to 37 °C for 30 min before mixing. Each DNA hairpin was heated to 95 °C for 5 min and then allowed to cool to room temperature for at least 2 h before use. In a typical protocol, all the assays were prepared in reaction buffer (10 mM Tris-HCl, 1 M NaCl, 50 mM $MgCl_2$, pH 7.5), the amplification reaction was carried out in a total volume of 60 μL buffer solution by mixing 30 μL target miRNA (varying concentrations) and 30 μL hairpin mix, which contained 0.10 μM of H1 and H2, 0.50 μM of H3 and H4, 0.50 μM of DNA reporter. The reaction mixture was then incubated at 37 °C for 1 h, and the emission spectra were recorded by exciting the samples at 491 nm from 510 to 600 nm.

Gel electrophoresis analysis

2% Agarose gels were prepared using 1× TBE buffer (89 mM Tris, 89 mM borate acid, 2 mM EDTA, PH 8.3) and 1× SYBR gel stain. Then 10 μL of different reaction products with loading buffer (5 : 1, v/v) were added to each well. Electrophoresis was run at 100 V for 70 min in 1× TBE buffer at room temperature, and finally the agarose gels were scanned and recorded by E-Gel Imager system (Invitrogen, USA).

Digital chip fabrication

The digital assay chip was composed of a layer of silicone elastomer PDMS bonded to a microscope glass slide. The microwell array photomask (~13 μm in diameter) was printed on a transparency film by a high resolution printer (Fineline Imaging, USA). To fabricate the PDMS chip, first, the silicon wafer was subjected to piranha cleaning (H_2SO_4 & H_2O_2), and baked at 200 °C for 5 minutes on a hotplate to dehydrate the surface. Then, the photoresist layer was prepared by spin-coating SU8-50 onto silicon wafer (4000 rpm for 45 s) to create an approximately ~13 μm high mold. After the silicon wafer (with photoresist layer) was soft baked at 65 °C for 5 min and 95 °C for 15 min, a film mask was used to align on the top of the silicon wafer and then exposed by ultraviolet light. The wafer was then post-baked at 65 °C for 1 min and 95 °C for 6 min. After dipping in the Microchem's SU8 developer for 10 min, the silicon wafer with microwell mold was washed with isopropyl alcohol (IPA) and dried with a gentle stream of air. This wafer was then used as the master template to fabricate a series of identical PDMS chips by adding silicone elastomer base and curing agent (10 : 1, w/w) onto the mold and heating to 70 °C for 40 min.

The dimension of the fabricated PDMS chip is ~10 mm × 10 mm, which contains 3 × 3 arrays of 100 × 100 individual wells (2 pL per well). For the digital assay, the glass slide was cleaned by piranha solution and then dried with the airflow. 2 μL of the hairpin mix was added to the center of the glass slide, then 2 μL sample solution was added to mix with the hairpin solution and subsequently sealed by the PDMS layer.

Digital assay quantification

The probability of a single-molecule occupancy in each microwell can be described by the Poisson distribution (eqn (1)),[57,58] where λ is the average number of analytes per well (*i.e.*, λ = (# of analytes)/(# of microwells)), and κ is the possible number of analytes per well.

$$P(k) = e^{-\lambda}\frac{\lambda^k}{k!} \quad (1)$$

The probability of forming negative wells (*i.e.*, "off" wells containing zero miR-21) in the microarray can be described by:

$$P(k = 0) = e^{-\lambda} \quad (2)$$

Accordingly, the probability of positive wells (*i.e.*, "on" wells containing at least one miRNA target) is:

$$P(k > 0) = 1 - P(k = 0) = 1 - e^{-\lambda} \quad (3)$$

The positive fraction f can then be expressed by:

$$f = 1 - e^{-\lambda} = 1 - e^{-v\ c\ x_{dil}N} \quad (4)$$

where v is the volume of microwell (2 pL), c is the concentration of miRNA (pM), x_{dil} is the diluted factor, and N is the Avogadro's number. For a given reaction volume and dilution factor, the concentration of miRNA will be eventually proportional to the number of positive wells, which can be described by:

$$-\ln(1 - f) = v\ c\ x_{dil}N \quad (5)$$

The positive wells were digitally counted by the Image pro plus (IPP) 6.0 software (Media Cybernetics, Inc., USA). To do that, the digital assay chip was first imaged by an inverted fluorescence microscope (Fig. S7A). The contrast of the images was then enhanced by increasing the brightness of the positive wells (Fig. S7B). Finally, the number of bright spots was automatically counted (Fig. S7C).

qPCR amplification

The concentration of miR-21 was detected using a two-step process:[59] First, the stem-loop RT primer was designed to

hybridize with the miR-21, and then reverse transcribed in a pulsed RT reaction. 5 μL miRNA was mixed with 5 μL of RT solution to 10 μL reaction volume, which contained 1 × RT buffer, 50 nM stem-loop RT primer, 250 μM dNTPs, and 3.33 U μL^{-1} reverse transcriptase. The reaction mixture was then incubated for 30 min at 16 °C, 30 min at 42 °C, 5 min at 85 °C and then held at 4 °C. Then the RT product was used for the PCR amplification: 1 μL of RT products were added into 24 μL of solution which contains 1 × PCR buffer, 200 μM dNTPs, 3 U of Taq DNA polymerase, 400 nM of Forward primer, 400 nM of Reverse primer, 18 mM $MgCl_2$, 0.1 mg ml^{-1} BSA, and 1 × SYBR Green dye. PCR was carried out using a thermal cycler with the following program: 94 °C for 4 min; 30 cycles at 94 °C for 30 s, 56 °C for 30 s, and 72 °C for 30 s; 72 °C for 5 min and finally 4 °C.

miR-21 detection in human serum and dry reagent testing

Human serum was diluted 10, 20, and 50 times before being spiked with miR-21 at different concentrations. Samples were then quantified by both analog and digital assays. For the dry reagent testing, the hairpin mix was first dried in a 96-well plate or on glass substrates, and rehydrated again when the sample was introduced. The rest reaction conditions are the same as the solution-based assay.

Quantification of miRNA in CRC samples

The serum samples from 9 CRC patients were provided by Duke University, Durham. Written informed consent was obtained from each patient regarding the use of plasma for this correlative analysis. This study was institutional review board (IRB) approved and registered with **https://www.clinicaltrials.gov** (study number: NC-T00597506). This retrospective analysis conforms to the reporting guidelines established by the REMARK criteria. All samples from CRC patients and healthy donors were treated by a protein denaturation protocol before being added to the dSENA chip reaction system. Briefly, 80 μL of 1 × PBS was added to 20 μL of serum sample, and the solution was heated to 95 °C for 5 min. Then the solution was cooled rapidly to 4 °C and kept for 3 min. Then the denatured serum lysates were centrifuged at 14000 rpm for 30 min at 4 °C. Finally, 2 μL of the supernatant was added to the reagent reaction system.

Author contributions

T. Y. and Q. W. designed and initiated the project. T. Y., A. D. P., A. H., S. Z., Z. L., and W. M. performed the experiments and collected the data. Y. L. and A. B. N. provided the clinical samples and validation results *via* RT-PCR. T. Y. and A. D. P. analyzed the data. T. Y and Q. W. wrote the manuscript. All the authors revised the manuscript and approved the submission.

Conflicts of interest

The authors declare no competing financial interest.

Data availability

The Supporting Information is available free of charge on the ACS Publications website. Sequences of the DNA and RNA used in this work; the fluorescence response, LOD, and amplification power of the CHA reaction; the calibration of fluorescent intensity *versus* the number of signal molecules; the amplification power of the SENA reaction; the comparison of the sealing with/without oxygen plasma treatment; fluorescence images processing and positive well counting; the theoretical result calculated from Poisson statistics; the recovery results of digital and analog assay results of dry reagents; the digital image of miR-21 detection with the CRC patient samples. See DOI: **https://doi.org/10.1039/D5SD00057B**.

The data supporting this article have been included as part of the ESI.

Ethical statement

Written informed consent was obtained from each patient regarding the use of plasma for this correlative analysis. This study was institutional review board (IRB) approved and registered with **https://www.clinicaltrials.gov** (study number: NC-T00597506). This retrospective analysis conforms to the reporting guidelines established by the REMARK criteria.

Acknowledgements

The authors greatly thank the start-up funds provided by NC State to perform the above research study.

References

1 D. P. Bartel, MicroRNAs: genomics, biogenesis, mechanism, and function, *Cell*, 2004, **116**(2), 281–297.
2 Z. Jin, D. Geissler, X. Qiu, K. D. Wegner and N. Hildebrandt, A Rapid, Amplification-Free, and Sensitive Diagnostic Assay for Single-Step Multiplexed Fluorescence Detection of MicroRNA, *Angew. Chem., Int. Ed.*, 2015, **54**(34), 10024–10029.
3 J. Li, S. Tan, R. Kooger, C. Zhang and Y. Zhang, MicroRNAs as novel biological targets for detection and regulation, *Chem. Soc. Rev.*, 2014, **43**(2), 506–517.
4 M. de Planell-Saguer and M. C. Rodicio, Detection methods for microRNAs in clinic practice, *Clin. Biochem.*, 2013, **46**(10–11), 869–878.
5 H. Schwarzenbach, N. Nishida, G. A. Calin and K. Pantel, Clinical relevance of circulating cell-free microRNAs in cancer, *Nat. Rev. Clin. Oncol.*, 2014, **11**(3), 145–156.
6 M. H. Mo, L. Chen, Y. Fu, W. Wang and S. W. Fu, Cell-free Circulating miRNA Biomarkers in Cancer, *J. Cancer*, 2012, **3**, 432–448.
7 H. Schwarzenbach, D. S. Hoon and K. Pantel, Cell-free nucleic acids as biomarkers in cancer patients, *Nat. Rev. Cancer*, 2011, **11**(6), 426–437.

8 G. S. Pall and A. J. Hamilton, Improved northern blot method for enhanced detection of small RNA, *Nat. Protoc.*, 2008, **3**(6), 1077–1084.
9 T. D. Schmittgen, E. J. Lee, J. Jiang, A. Sarkar, L. Yang, T. S. Elton and C. Chen, Real-time PCR quantification of precursor and mature microRNA, *Methods*, 2008, **44**(1), 31–38.
10 C. Chen, D. A. Ridzon, A. J. Broomer, Z. Zhou, D. H. Lee, J. T. Nguyen, M. Barbisin, N. L. Xu, V. R. Mahuvakar, M. R. Andersen, K. Q. Lao, K. J. Livak and K. J. Guegler, Real-time quantification of microRNAs by stem-loop RT-PCR, *Nucleic Acids Res.*, 2005, **33**(20), e179.
11 Z. Y. Wang, M. H. Sun, Q. Zhang, P. F. Li, K. Wang and X. M. Li, Advances in Point-of-Care Testing of microRNAs Based on Portable Instruments and Visual Detection, *Biosensors*, 2023, **13**(7), 747.
12 W. Wang, Q. Ge and X. Zhao, Enzyme-Free Isothermal Amplification Strategy for the Detection of Tumor-Associated Biomarkers: A Review, *TrAC, Trends Anal. Chem.*, 2023, **160**, 116960.
13 N. O. Prado, A. M. Marin and L. A. Lalli, *et al.*, Development and Evaluation of a Lyophilization Protocol for Colorimetric RT-LAMP Diagnostic Assay for COVID-19, *Sci. Rep.*, 2024, **14**, 10612.
14 T. C. Lorenz, Polymerase Chain Reaction: Basic Protocol plus Troubleshooting and Optimization Strategies, *J. Visualized Exp.*, 2012, **63**, e3998.
15 J. Lei and H. Ju, Signal amplification using functional nanomaterials for biosensing, *Chem. Soc. Rev.*, 2012, **41**(6), 2122–2134.
16 Y. Sun, L. Shi, Q. Wang, L. Mi and T. Li, Spherical Nucleic Acid Enzyme (SNAzyme) Boosted Chemiluminescence miRNA Imaging Using a Smartphone, *Anal. Chem.*, 2019, **91**(5), 3652–3658.
17 J. Mandli, H. Mohammadi and A. Amine, Electrochemical DNA sandwich biosensor based on enzyme amplified microRNA-21 detection and gold nanoparticles, *Bioelectrochemistry*, 2017, **116**, 17–23.
18 N. Zhang, X. M. Shi, H. Q. Guo, X. Z. Zhao, W. W. Zhao, J. J. Xu and H. Y. Chen, Gold Nanoparticle Couples with Entropy-Driven Toehold-Mediated DNA Strand Displacement Reaction on Magnetic Beads: Toward Ultrasensitive Energy-Transfer-Based Photoelectrochemical Detection of miRNA-141 in Real Blood Sample, *Anal. Chem.*, 2018, **90**(20), 11892–11898.
19 Z. Ge, M. Lin, P. Wang, H. Pei, J. Yan, J. Shi, Q. Huang, D. He, C. Fan and X. Zuo, Hybridization chain reaction amplification of microRNA detection with a tetrahedral DNA nanostructure-based electrochemical biosensor, *Anal. Chem.*, 2014, **86**(4), 2124–2130.
20 T. Kilic, A. Erdem, M. Ozsoz and S. Carrara, microRNA biosensors: Opportunities and challenges among conventional and commercially available techniques, *Biosens. Bioelectron.*, 2018, **99**, 525–546.
21 Y. L. Zhu, Y. M. Lian, J. K. Wang, Z. P. Chen and R. Q. Yu, Highly Sensitive and Specific Mass Spectrometric Platform for miRNA Detection Based on the Multiple-Metal-Nanoparticle Tagging Strategy, *Anal. Chem.*, 2021, **93**(14), 5839–5848.
22 Y. Zang, J. Lei, P. Ling and H. Ju, Catalytic Hairpin Assembly-Programmed Porphyrin-DNA Complex as Photoelectrochemical Initiator for DNA Biosensing, *Anal. Chem.*, 2015, **87**(10), 5430–5436.
23 A. Karunanayake Mudiyanselage, Q. Yu, M. A. Leon-Duque, B. Zhao, R. Wu and M. You, Genetically Encoded Catalytic Hairpin Assembly for Sensitive RNA Imaging in Live Cells, *J. Am. Chem. Soc.*, 2018, **140**(28), 8739–8745.
24 Y. S. Jiang, B. Li, J. N. Milligan, S. Bhadra and A. D. Ellington, Real-time detection of isothermal amplification reactions with thermostable catalytic hairpin assembly, *J. Am. Chem. Soc.*, 2013, **135**(20), 7430–7433.
25 D. Kim, Q. Wei, D. H. Kim, D. Tseng, J. Zhang, E. Pan, O. Garner, A. Ozcan and D. Di Carlo, Enzyme-Free Nucleic Acid Amplification Assay Using a Cellphone-Based Well Plate Fluorescence Reader, *Anal. Chem.*, 2018, **90**(1), 690–695.
26 C. Jung and A. D. Ellington, Diagnostic applications of nucleic acid circuits, *Acc. Chem. Res.*, 2014, **47**(6), 1825–1835.
27 J. Wei, X. Gong, Q. Wang, M. Pan, X. Liu, J. Liu, F. Xia and F. Wang, Construction of an autonomously concatenated hybridization chain reaction for signal amplification and intracellular imaging, *Chem. Sci.*, 2018, **9**(1), 52–61.
28 H. Wang, C. Li, X. Liu, X. Zhou and F. Wang, Construction of an enzyme-free concatenated DNA circuit for signal amplification and intracellular imaging, *Chem. Sci.*, 2018, **9**(29), 5842–5849.
29 J. Guo, C. Mingoes, X. Qiu and N. Hildebrandt, Simple, Amplified, and Multiplexed Detection of MicroRNAs Using Time-Gated FRET and Hybridization Chain Reaction, *Anal. Chem.*, 2019, **91**(4), 3101–3109.
30 Y. Wei, W. Zhou, X. Li, Y. Chai, R. Yuan and Y. Xiang, Coupling hybridization chain reaction with catalytic hairpin assembly enables non-enzymatic and sensitive fluorescent detection of microRNA cancer biomarkers, *Biosens. Bioelectron.*, 2016, **77**, 416–420.
31 C. Feng, J. Zhu, J. Sun, W. Jiang and L. Wang, Hairpin assembly circuit-based fluorescence cooperative amplification strategy for enzyme-free and label-free detection of small molecule, *Talanta*, 2015, **143**, 101–106.
32 Q. Wang, M. Pan, J. Wei, X. Liu and F. Wang, Evaluation of DNA Methyltransferase Activity and Inhibition via Isothermal Enzyme-Free Concatenated Hybridization Chain Reaction, *ACS Sens.*, 2017, **2**(7), 932–939.
33 H. Cheng, W. Li, S. Duan, J. Peng, J. Liu, W. Ma, H. Wang, X. He and K. Wang, Mesoporous Silica Containers and Programmed Catalytic Hairpin Assembly/Hybridization Chain Reaction Based Electrochemical Sensing Platform for MicroRNA Ultrasensitive Detection with Low Background, *Anal. Chem.*, 2019, **91**(16), 10672–10678.
34 B. Li, Y. Jiang, X. Chen and A. D. Ellington, Probing spatial organization of DNA strands using enzyme-free hairpin assembly circuits, *J. Am. Chem. Soc.*, 2012, **134**(34), 13918–13921.
35 X. Chen, N. Briggs, J. R. McLain and A. D. Ellington, Stacking nonenzymatic circuits for high signal gain, *Proc. Natl. Acad. Sci. U. S. A.*, 2013, **110**(14), 5386–5391.
36 K. Quan, J. Huang, X. Yang, Y. Yang, L. Ying, H. Wang, N. Xie, M. Ou and K. Wang, Powerful Amplification Cascades of

FRET-Based Two-Layer Nonenzymatic Nucleic Acid Circuits, *Anal. Chem.*, 2016, **88**(11), 5857–5864.
37 H. Wang, C. Li, X. Liu, X. Zhou and F. Wang, Construction of an Enzyme-Free Concatenated DNA Circuit for Signal Amplification and Intracellular Imaging, *Chem. Sci.*, 2018, **9**, 5842–5849.
38 C. Li, J. Zhang, Y. Gao, S. Luo and Z. S. Wu, Nonenzymatic Autonomous Assembly of Cross-Linked Network Structures from Only Two Palindromic DNA Components for Intracellular Fluorescence Imaging of miRNAs, *ACS Sens.*, 2022, **7**, 601–611.
39 Y. Wei, W. Zhou, X. Li, Y. Chai, R. Yuan and Y. Xiang, Coupling Hybridization Chain Reaction with Catalytic Hairpin Assembly Enables Non-Enzymatic and Sensitive Fluorescent Detection of microRNA Cancer Biomarkers, *Biosens. Bioelectron.*, 2016, **77**, 416–420.
40 T. Li, T. S. Lau, J. Li, K. Hu, M. L. Lee, P. Y. Chen, C. C. Wang and H. W. Li, Programmable PCR-Like Nonenzymatic DNA Molecular Circuit for Split-Free Autocatalytic Amplification, *Anal. Chem.*, 2025, **97**(22), 11847–11855.
41 Y. Rondelez, G. Tresset, K. V. Tabata, H. Arata, H. Fujita, S. Takeuchi and H. Noji, Microfabricated arrays of femtoliter chambers allow single molecule enzymology, *Nat. Biotechnol.*, 2005, **23**(3), 361–365.
42 A. S. Basu, Digital Assays Part I: Partitioning Statistics and Digital PCR, *SLAS Technol.*, 2017, **22**(4), 369–386.
43 J. E. Kreutz, T. Munson, T. Huynh, F. Shen, W. Du and R. F. Ismagilov, Theoretical design and analysis of multivolume digital assays with wide dynamic range validated experimentally with microfluidic digital PCR, *Anal. Chem.*, 2011, **83**(21), 8158–8168.
44 J. S. Park, K. Hsieh, L. Chen, A. Kaushik, A. Y. Trick and T. H. Wang, Digital CRISPR/Cas-Assisted Assay for Rapid and Sensitive Detection of SARS-CoV-2, *Adv. Sci.*, 2021, **8**(5), 2003564.
45 Y. Men, Y. Fu, Z. Chen, P. A. Sims, W. J. Greenleaf and Y. Huang, Digital polymerase chain reaction in an array of femtoliter polydimethylsiloxane microreactors, *Anal. Chem.*, 2012, **84**(10), 4262–4266.
46 F. Shen, B. Sun, J. E. Kreutz, E. K. Davydova, W. Du, P. L. Reddy, L. J. Joseph and R. F. Ismagilov, Multiplexed quantification of nucleic acids with large dynamic range using multivolume digital RT-PCR on a rotational SlipChip tested with HIV and hepatitis C viral load, *J. Am. Chem. Soc.*, 2011, **133**(44), 17705–17712.
47 A. C. Hatch, J. S. Fisher, A. R. Tovar, A. T. Hsieh, R. Lin, S. L. Pentoney, D. L. Yang and A. P. Lee, 1-Million droplet array with wide-field fluorescence imaging for digital PCR, *Lab Chip*, 2011, **11**(22), 3838–3845.
48 P. D. R. Cirillo, K. Margiotti, A. Mesoraca and C. Giorlandino, Quantification of circulating microRNAs by droplet digital PCR for cancer detection, *BMC Res. Notes*, 2020, **13**(1), 351.
49 X. Lin, X. Huang, Y. Zhu, K. Urmann, X. Xie and M. R. Hoffmann, Asymmetric Membrane for Digital Detection of Single Bacteria in Milliliters of Complex Water Samples, *ACS Nano*, 2018, **12**(10), 10281–10290.
50 J. Rodriguez-Manzano, M. A. Karymov, S. Begolo, D. A. Selck, D. V. Zhukov, E. Jue and R. F. Ismagilov, Reading Out Single-Molecule Digital RNA and DNA Isothermal Amplification in Nanoliter Volumes with Unmodified Camera Phones, *ACS Nano*, 2016, **10**(3), 3102–3113.
51 T. D. Rane, L. Chen, H. C. Zec and T. H. Wang, Microfluidic continuous flow digital loop-mediated isothermal amplification (LAMP), *Lab Chip*, 2015, **15**(3), 776–782.
52 K. Leirs, P. Tewari Kumar, D. Decrop, E. Perez-Ruiz, P. Leblebici, B. Van Kelst, G. Compernolle, H. Meeuws, L. Van Wesenbeeck, O. Lagatie, L. Stuyver, A. Gils, J. Lammertyn and D. Spasic, Bioassay Development for Ultrasensitive Detection of Influenza A Nucleoprotein Using Digital ELISA, *Anal. Chem.*, 2016, **88**(17), 8450–8458.
53 D. M. Rissin, C. W. Kan, T. G. Campbell, S. C. Howes, D. R. Fournier, L. Song, T. Piech, P. P. Patel, L. Chang, A. J. Rivnak, E. P. Ferrell, J. D. Randall, G. K. Provuncher, D. R. Walt and D. C. Duffy, Single-molecule enzyme-linked immunosorbent assay detects serum proteins at subfemtomolar concentrations, *Nat. Biotechnol.*, 2010, **28**(6), 595–599.
54 D. Kim, O. B. Garner, A. Ozcan and D. Di Carlo, Homogeneous Entropy-Driven Amplified Detection of Biomolecular Interactions, *ACS Nano*, 2016, **10**(8), 7467–7475.
55 W. E. Arter, Y. Yusim, Q. Peter, C. G. Taylor, D. Klenerman, U. F. Keyser and T. P. J. Knowles, Digital Sensing and Molecular Computation by an Enzyme-Free DNA Circuit, *ACS Nano*, 2020, **14**(5), 5763–5771.
56 N. V. Conev, I. S. Donev, A. A. Konsoulova-Kirova, T. G. Chervenkov, J. K. Kashlov and K. D. Ivanov, Serum expression levels of miR-17, miR-21, and miR-92 as potential biomarkers for recurrence after adjuvant chemotherapy in colon cancer patients, *BioSci. Trends*, 2015, **9**(6), 393–401.
57 K. Schee, O. Fodstad and K. Flatmark, MicroRNAs as biomarkers in colorectal cancer, *Am. J. Pathol.*, 2010, **177**(4), 1592–1599.
58 T. Gou, J. Hu, W. Wu, X. Ding, S. Zhou, W. Fang and Y. Mu, Smartphone-based mobile digital PCR device for DNA quantitative analysis with high accuracy, *Biosens. Bioelectron.*, 2018, **120**, 144–152.
59 E. Varkonyi-Gasic, R. Wu, M. Wood, E. F. Walton and R. P. Hellens, Protocol: a highly sensitive RT-PCR method for detection and quantification of microRNAs, *Plant Methods*, 2007, **3**, 12.